lubricants

MDPI

Article

Influence of Circumferential Convergent Wedge Pocket on the Segmented Annular Seal's Static and Dynamic Characteristics

Shuang Wang [1,2], Dan Sun [1,2,*], Zemin Yang [1,2], Wenfeng Xu [1,2] and Huan Zhao [1,2]

[1] Key Lab of Advanced Test Technology for Aerospace Propulsion System, Shenyang Aerospace University, Shenyang 110136, China
[2] Key Laboratory of Turbomachinery Advanced Seal Technology, Shenyang Aerospace University, Shenyang 110136, China
* Correspondence: phd_sundan@email.sau.edu.cn or phd_sundan@163.com

Abstract: Aiming at the problem of abnormal wear caused by the poor dynamic characteristics of aeroengine segmented annular seals, according to the hydrodynamic lubrication theory, based on the conventional structure featuring the Rayleigh step profile rectangular pocket (RP), novel structures with the circumferential linear convergent pocket (CLCP) and the circumferential parabolic convergent pocket (CPCP) were proposed. A model was developed to analyze both the static and dynamic characteristics of three types of segmented annular seals, utilizing the local differential quadrature (LDQ) method. Once the accuracy of the solution model was confirmed, the effects of working conditions and design features on both static and dynamic characteristics were analyzed. Results indicate that the circumferential wedge convergent pockets can effectively improve the dynamic characteristics of the seal system. Under different rotational speeds, compared with the RP seal, the CLCP seal's stiffness coefficient and damping coefficient increases by an average of 60.76% and 65.27%, respectively. As the rotational speed increases, the RP seal damping ratio decreases, and the seal system transitions from an overdamped state to an underdamped state, resulting in reduced stability. Nevertheless, under different rotational speeds and pressure ratios, the CLCP and the CPCP seals are both in an overdamped state. Taking into account the static and dynamic characteristics, the CLCP seal is the optimal structure in this study.

Keywords: circumferential convergent wedge pocket; segmented annular seal; static characteristics; dynamic characteristics

check for updates

Received: 12 January 2025
Revised: 17 February 2025
Accepted: 24 February 2025
Published: 12 March 2025

Citation: Wang, S.; Sun, D.; Yang, Z.; Xu, W.; Zhao, H. Influence of Circumferential Convergent Wedge Pocket on the Segmented Annular Seal's Static and Dynamic Characteristics. *Lubricants* **2025**, *13*, 121. https://doi.org/10.3390/lubricants13030121

Copyright: © 2025 by the authors. Licensee MDPI, Basel, Switzerland. This article is an open access article distributed under the terms and conditions of the Creative Commons Attribution (CC BY) license (https://creativecommons.org/licenses/by/4.0/).

1. Introduction

A segmented annular seal is a critical component in aeroengines, primarily served as a seal for lubricating oil within the bearing chamber. With the continuous development of aeroengines toward high parameters, the segmented annular seal encounters significant challenges, including abnormal wear caused by poor dynamic characteristics while reducing leakage [1–3]. Surface micro-textures can improve the lubrication performance of seal friction pairs and rotor stability, so the micro-textured design of the friction interface in segmented annular seals has emerged as a focal point of research [4]. Consequently, studying the new micro-textured segmented annular seal's static and dynamic characteristics has important scientific significance and engineering application value.

In 1967, NASA first employed segmented annular seals for gas and liquid sealing [5] and utilized two seals mentioned above for the helium sealing of the oxygen turbopump in the J-2 engine [6]. PW and Stein in the USA considered the segmented annular seal without

micro-textures as the preferred sealing type for the bearing chamber of gear transmission fan engines [7]. Ludwig applied segmented annular seals to small gas turbine engines. The results indicate that compared to rotational speed, the influence of pressure difference on leakage is more significant [8]. Bai et al. [9] employed the finite difference method to solve the Reynolds equation for the segmented annular seal. The results indicate that the waviness can generate fluid hydrodynamic pressure effects. The segmented annular seals mentioned above are all seals without micro-textures. Their hydrodynamic pressure effect generated by waviness is weak [10], resulting in abnormal wear caused by insufficient lift force and poor dynamic characteristics, leading to faults such as oil leakage in the bearing chamber [11].

It has been demonstrated that surface micro-texturing enhances the lubrication performance and dynamic characteristics of seal frictional pairs [12]. The micro-texturing of the friction interface of segmented annular seals has become a research hotspot. In the 1970s, NASA initiated micro-texture designs for segmented annular seals [13] and designed rectangular pockets that facilitate the generation of hydrodynamic pressure effects. This structural design proposal reduces contact loads on the sealing surface and improves sealing performance. Subsequently, both NASA [14–16] and JAXA [17,18] demonstrated that rectangular pockets can reduce sealing surface wear, determine the magnitude of the segment lift force, and minimize the seal leakage of the seal in a non-contact state. Yuri and colleagues [19] employed the finite element method for the numerical solution of the Reynolds equation pertaining to a segmented annular seal and conducted a theoretical investigation of how spherical micro-texture influences the mean lift pressure of the seal segment. The findings reveal that the hydrodynamic pressure generated by spherical micro-textures within the seal clearance can elevate the average lift pressure of the seal by 50% above the ambient pressure. Sun et al. [20] used the local differential quadrature algorithm to numerically analyze the impact of pocket design parameters on the pressure distribution of segmented annular seals. The findings of the research indicate that an increase in pocket length leads to a rise in pressure peaks, while an increase in pocket depth and width initially raises the pressure peaks before causing them to decrease. Arghir et al. [10] employed the finite volume method to numerically solve the segmented annular seal Reynolds equation, examining the impact of the geometric scheme as well as the operating conditions on fluid leakage. The findings suggest that the dimensions of the pocket, both length and width, have a negligible effect on leakage. Afterwards, the scholars in the study team compared and analyzed the impact of the compression number on the seal lift force of [21]. The research results indicate that under high-pressure compression conditions, segmented annular seals with inclined micro-textures have greater lift force. The segmented annular seals with the above micro-textures can enhance the hydrodynamic pressure effect, but there are still problems such as the insufficient hydrodynamic pressure effect and poor dynamic characteristics, leading to seal wear failure [9]. For the sake of evaluating the segmented annular seal dynamic characteristics, Sun et al. [22] applied the differential quadrature method to numerically analyze the impact of pocket design parameters on the seal dynamic characteristics. The findings reveal that an increase in the rectangular pocket depth and width initially boosts both of the dynamic characteristic coefficients before causing them to decrease. An increase in pocket length leads to higher stiffness and damping coefficients. In summary, the micro-texture configurations in existing studies on the static and dynamic characteristics of the segmented annular seal are all rectangular. However, the segmented annular seal with rectangular micro-textures still suffers from the problem of segment wear caused by poor dynamic characteristics. Although scholars such as Li et al. [23,24] have attempted to improve the sealing performance by proposing new anti-fishbone micro-textures and diagonal micro-textures to optimize the

shape of micro-textures, the structural innovations above have not considered the influence of micro-textures on the dynamic characteristics of segmented annular seals. Hence, the influence of micro-texture optimization design on the dynamic characteristics of segmented annular seals has not been fully studied at present. This article systematically analyzes the influence of a wedge-shaped micro-texture, a new type of micro-texture, on the static and dynamic characteristics of segmented annular seals, and improves the research on the influence of micro-textures on the static and dynamic characteristics of segmented annular seals in this field.

In response to the above problems, according to the hydrodynamic lubrication theory, the segmented annular seal structure with the circumferential linear convergent pocket and the circumferential parabolic convergent pocket improves the RP seal dynamic characteristics. A numerical investigation was conducted utilizing the LDQ method to examine how working parameters and pocket structure affect the segmented annular seal's static and dynamic characteristics.

2. Design of Seal Structure with Circumferential Convergent Wedge Pockets

2.1. Configuration of the Segmented Annular Seal

Figure 1 illustrates the typical segmented annular seal structure. The seal components include segments, springs, and other elements. The segmented annular seal comprises a main seal surface and an auxiliary seal surface. The main sealing surface, located on the inner face of the segment, includes axial grooves, a circumferential groove used for guiding flow, as well as pockets that create hydrodynamic pressure effects. The medium flows in from the end face with axial grooves and flows out from the other end face. The auxiliary seal surface, located on the end face near the circumferential groove, is tightly pressed against the mounting end face by an axial spring to keep the seal in contact with the rotor.

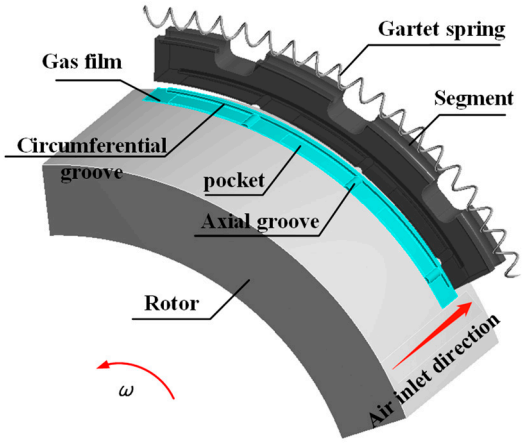

Figure 1. Structure of the segmented annular seal components.

2.2. Working Principle

Figure 2 displays the schematic diagram for analyzing the forces on the segmented annular seal. F_G, F_Z, F_0, F_c, F_f, and F_y stand for the lift force, the runway contact force, the closing force generated by the medium, the closing force generated by the garter spring, the friction force of the auxiliary seal surface, and the axial force generated by the axial spring and medium pressure, respectively.

After assembly, the segmented annular seal component is clamped onto the rotor under the action of the garter spring. The radial force balance expression of the segment is as follows:

$$F_z = F_0 + F_c \tag{1}$$

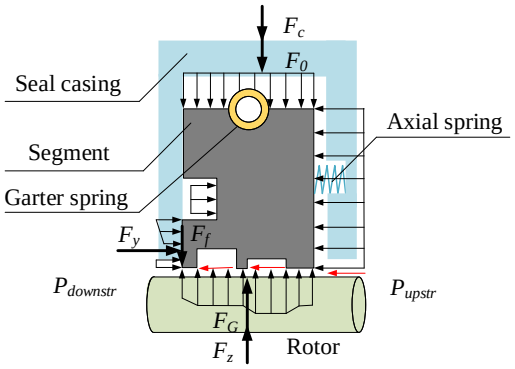

Figure 2. Forces acting on a segment.

The operation of a segmented annular seal can be divided into three states: starting up, working, and deceleration. During the start-up process, the fluid in the pocket is subjected to the circumferential velocity generated by the rotor rotation, forming the hydrodynamic pressure effect. The inner surface of the segment is subjected to a gradually increasing gas film force, leading to a gradual reduction in the contact force acting on the rotor, until it ultimately diminishes to zero. Simultaneously, the side of the segment is subjected to frictional force F_f. In this state, the radial force balance expression of the segment is as follows:

$$F_G + F_z = F_0 + F_c + F_f \tag{2}$$

As the rotational speed increases to the operational level, a stable clearance is formed between the segment and the rotor. The radial force balance expression of the segment is as follows:

$$F_G = F_0 + F_c \tag{3}$$

when the segmented annular seal is in a deceleration state, the force analysis of the segment is similar to the starting process, with the difference being the direction of the friction force. When the rotational speed approaches 0, the radial force balance expression of the segment is shown in Equation (1).

The existing RP seals exhibit a deficient hydrodynamic pressure effect and unsatisfactory dynamic characteristics. This ultimately results in the premature failure of the seals due to wear, which subsequently leads to oil leakage from the bearing chambers of the aeroengine.

2.3. Design of Seal with Circumferential Convergent Wedge Pocket

A segmented annular seal is a typical hydrodynamic pressure-type seal. The microtexture at the circumferential outlet of the sealed gas film clearance meets the necessary conditions for forming hydrodynamic pressure gas film: (1) a wedge-shaped clearance is formed between the rotor and the stator; (2) the rotor and stator are continuously filled with viscous flow; (3) there is relative velocity between the rotor and the stator, causing the fluid to move from the large end of the clearance to the small end of the clearance to form a convergent wedge-shaped flow field. The wedge-shaped clearance is a key structure that forms hydrodynamic pressure effects and improves the dynamic characteristics of the segmented annular seals.

In response to the problem of the inadequate hydrodynamic lubrication effect and dynamic characteristics, a novel segmented annular seal structure with a circumferential convergent wedge pocket was proposed, as shown in Figure 3. In the figure, R, c, and h_1 represent the seal radius, seal clearance, and the maximum depth of the circumferential convergent wedge pocket, respectively. The rotor rotation causes fluid to flow from the

large clearance position ($R + c + h_1$) into the small clearance position ($R + c$), forming a convergent wedge clearance to enhance the hydrodynamic pressure effect.

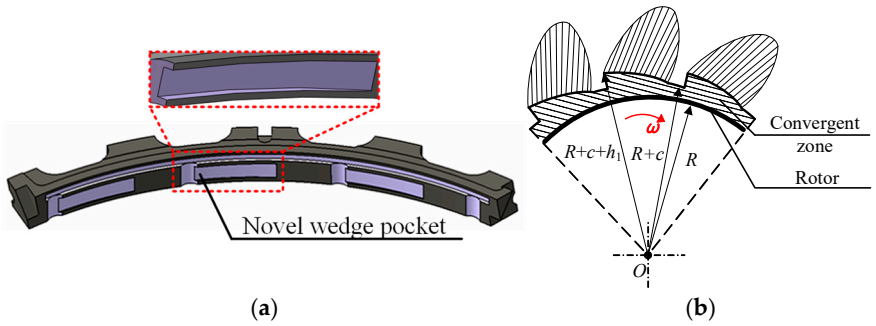

(**a**) (**b**)

Figure 3. Schematic diagram of the novel wedge pocket and the hydrodynamic pressure effect. (**a**) Schematic of the segment. (**b**) Schematic of the hydrodynamic effect.

Based on the RP seal, two types of seal structures with the CLCP and the CPCP were proposed, respectively. The schematic diagrams of the main sealing surface groove type, radial fluid film, and circumferential fluid film of the above three seals are shown in Figures 4–6.

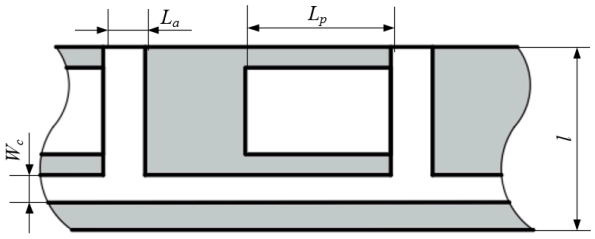

Figure 4. Schematic diagram of main sealing surface groove details.

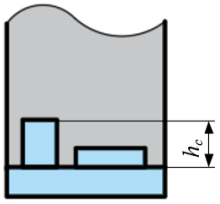

Figure 5. Schematic diagram of radial fluid film details.

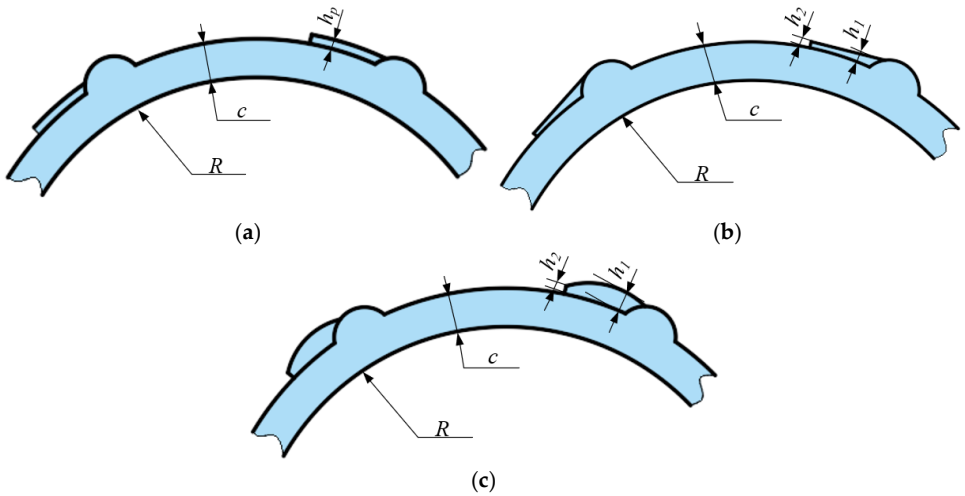

(**a**) (**b**)

(**c**)

Figure 6. Schematic diagram of circumferential fluid film details. (**a**) Traditional rectangular pocket. (**b**) Circumferential linear convergent pocket. (**c**) Circumferential parabolic convergent pocket.

3. Theoretical Model

3.1. Theoretical Model of Static and Dynamic Characteristics

3.1.1. Static Characteristics

According to the principle of fluid lubrication [24], assuming that the medium viscosity remains constant, the medium pressure satisfies the following Reynolds equation:

$$\frac{\partial}{\partial x}\left(\frac{\rho h^3}{12\eta}\frac{\partial p}{\partial x}\right)+\frac{\partial}{\partial y}\left(\frac{\rho h^3}{12\eta}\frac{\partial p}{\partial y}\right)=\frac{1}{2}\frac{\partial}{\partial x}(U\,\rho h) \tag{4}$$

The density and dynamic viscosity of the sealing medium are denoted by ρ and η, respectively. The velocity of the rotor is represented by U. The thickness of the gas film is given by h. The pressure of the medium is indicated by p. The coordinates x and y represent two directions in a Cartesian coordinate system.

The seal inlet and outlet adhere to the specified pressure, while its symmetrical edges comply with the periodic boundary conditions.

The formulas for calculating lift force and leakage are as follows:

$$F_G=\iint_A prl\mathrm{d}\theta\mathrm{d}\lambda \tag{5}$$

$$Q=-\int_0^{2\pi}\frac{\rho h^3}{12\eta}\frac{\partial p}{\partial \lambda}\frac{r}{l}\mathrm{d}\theta \tag{6}$$

3.1.2. Dynamic Characteristics

When the rotor navigates minor vortical disturbances around the stator's central axis, the sealing dynamic coefficients is as follows [25]:

$$\begin{bmatrix}\Delta F_x\\ \Delta F_y\end{bmatrix}=\begin{bmatrix}K_{xx} & K_{xy}\\ K_{yx} & K_{yy}\end{bmatrix}\begin{bmatrix}\Delta x\\ \Delta y\end{bmatrix}+\begin{bmatrix}C_{xx} & C_{xy}\\ C_{yx} & C_{yy}\end{bmatrix}\begin{bmatrix}\Delta \dot{x}\\ \Delta \dot{y}\end{bmatrix} \tag{7}$$

where K_{xx} and K_{yy} signify direct stiffness coefficients. K_{xy} and K_{yx} denote cross-stiffness coefficients. C_{xx} and C_{yy} represent direct-damping coefficients. C_{xy} and C_{yx} represent cross-damping coefficients. Δx and Δy are vortex displacements. $\Delta \dot{x}$ and $\Delta \dot{y}$ are vortex velocities.

When the segment experiences minor vortices, the dynamic characteristics can be defined as follows [22]:

$$\begin{cases} K_{rr}=\frac{\Delta F_r}{\Delta r}\\ C_{rr}=\frac{\Delta F_r}{\Delta \dot{r}}\end{cases} \tag{8}$$

Unlike the stability analysis of integral seals, the segment makes a similar simple harmonic vibration in only one direction. For a single segment, the segment and gas film can be regarded as a mass–spring–damping system, and the damping ratio of the system can be obtained as $\varsigma=\frac{C_{rr}}{2\sqrt{MK_{rr}}}$, where M is the mass of the segment.

For the unit step response:

(1) When $0<\varsigma<1$, the system is in an underdamped state. The system is stable.

(2) When $\varsigma\geq 1$, the system is in an overdamped state. The system demonstrates superior stability when compared to a system with an underdamped response.

(3) When $\varsigma\leq 0$, the system is unstable.

3.2. Static and Dynamic Characteristics Solution

Utilizing the above control equations and boundary conditions, employing the workflow depicted in Figure 7, the steps below can be followed to determine the segmented annular seal static and dynamic characteristics:

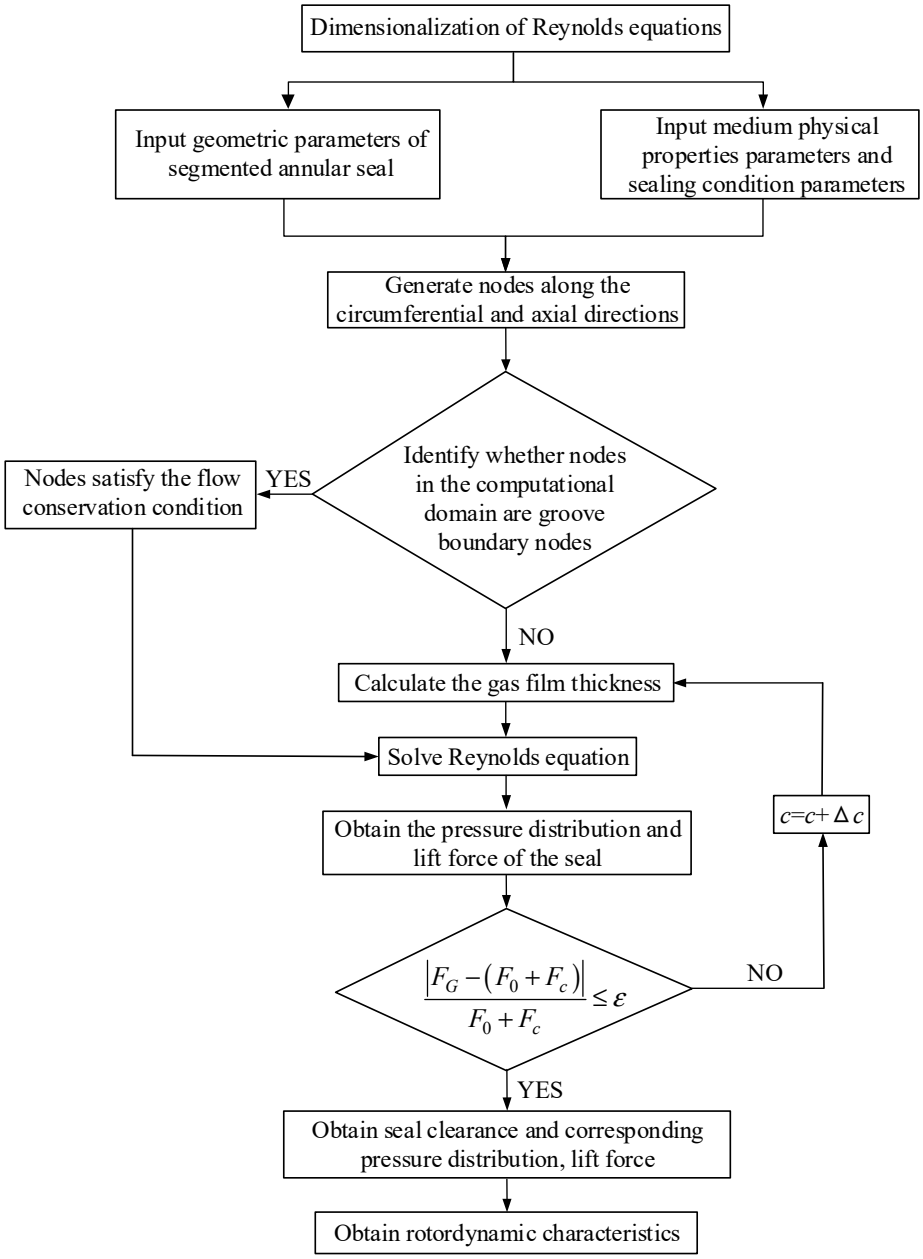

Figure 7. Calculation process for static and dynamic characteristics.

(1) Non-dimensionalize the Reynolds equation.

(2) Input the segmented annular seal geometric parameters, the medium physical properties, the working condition parameters, and the control equations satisfied by each node.

(3) Employ the local differential quadrature method [26] to discretize the Reynolds equation for the fluid within the sealing clearance. Utilize the least squares method to determine segmented annular seal pressure distribution and lift force at a particular clearance.

(4) Determine whether the relative error between the lift force and the closing force is less than or equal to the threshold. If this is the case, the clearance in question represents the actual seal clearance. Under these conditions, the leakage and dynamic characteristics can be attained. In the event that the aforementioned conditions are not met, it is necessary to adjust the sealing clearance and then repeat the process (3) several times to ensure that the relative error of the lift force and the closing force combined force is less than or equal to the specified threshold 10-6. As a result, the segmented annular seal static and dynamic characteristics that meet the working conditions can be obtained.

4. Analysis Model and Accuracy Verification of Computational Method

4.1. Geometric Configuration and Working Conditions

The basic structural dimensions of the segmented seal are detailed in [24]. In this paper, only the depth dimensions of the three types of pockets are given, as shown in Table 1. The working condition parameters used for the computational analysis are shown in Table 2.

Table 1. Key structure parameters of the segmented annular seal.

Item	Seal with the RP	Seal with the CLCP	Seal with the CPCP
Depth of RP/mm	0.015	—	—
Circumferential convergent pocket depth 1/mm	—	0.010	0.010
Circumferential convergent pocket depth 2/mm	—	0.025	0.025

Table 2. The segmented annular seal operating condition.

Item	Value	Item	Value
Rotational speed n/r·min^{-1}	3000~15,000	Outlet pressure p_0/MPa	0.10
Pressure ratio (*P.R.*)	3.30~3.45	Air dynamic viscosity/Pa·s	1.83×10^{-5}
Spring force F_s/N	0.36, 0.315		

4.2. Influence of Node Density on Results

To improve computational precision and efficiency, a verification of node independence was conducted, taking into account the leakage. The number of nodes with seven different densities in the computational domain were analyzed. The impact of the node number on the leakage of the segmented annular seals with three kinds of pockets is, respectively, illustrated in Figure 8. With the rise in node count, the segmented annular seal initially exhibits increased leakage before stabilizing. When the node number reaches or exceeds 10,560, the relative error of leakage is less than 5%. For the sake of calculation accuracy and efficiency, the number of nodes for this study is 10,560.

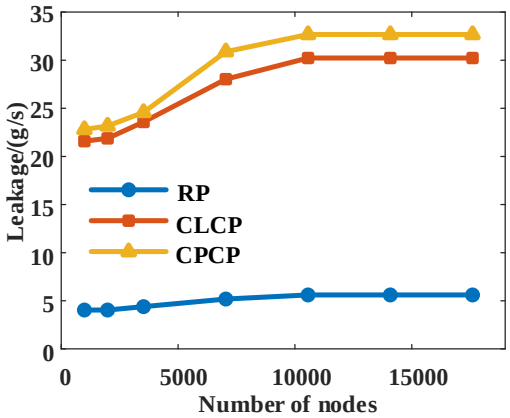

Figure 8. Impact of node number on leakage (p_0 = 0.1 MPa, *P.R.* = 4, n = 15,000 r·min^{-1}).

4.3. Calculation Method Accuracy Verification

To confirm the computational method's precision, the RP seal leakage was chosen to compare with the experimental results. In addition, the method accuracy for the dynamic characteristics of the RP seal was verified.

4.3.1. Experimental Validation of Leakage Characteristics' Calculation Methods

The experimental platform for segmented annular seal leakage comprises an oil supply system, a gas supply system, a testing system, and a power system. Initially, the gas from the compressor enters the storage tank, subsequently proceeds to the sealing chamber, and ultimately discharges into the environment. The experimental rig's primary experimental parts are motor, rotor runway, support seat, test box, seal chamber, end cover, segmented annular seal test piece, and oil injection pipe. The physical image of the experimental platform is shown in Figure 9. The seal test piece's physical picture is illustrated in Figure 10.

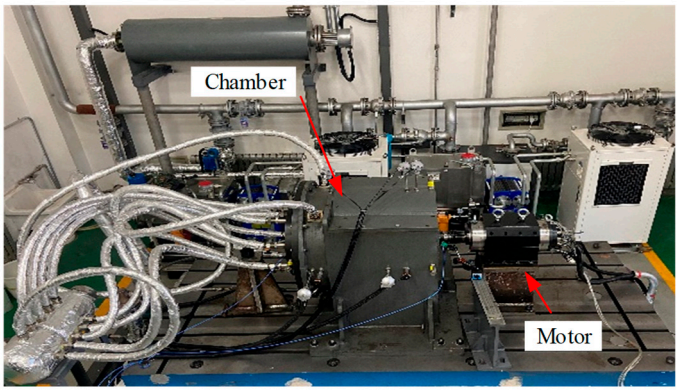

Figure 9. Experimental rig.

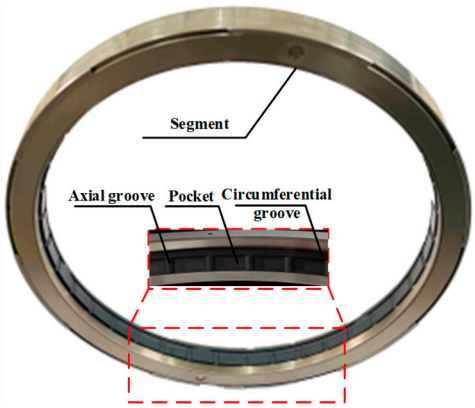

Figure 10. Test piece's physical picture.

Figure 11 presents a diagram illustrating the segmented annular seal leakage test. The seal's high-pressure side features both inlet and outlet ducts. A high-precision EPI flow meter, with a measuring range of 35 m^3/h and a measurement accuracy of 1%, was installed in each of the inlet and outlet ducts. The distinction between the two meters is the segmented annular seal leakage. It is necessary to adjust the status of the inlet regulating valve in order to regulate the inlet pressure. Additionally, it is essential to ensure the pressure ratio across the experimental components remains within the defined error range, while monitoring the sensor feedback signal. Once the pressure ratio has reached a stable state, the power system should be activated, and the segmented annular seal leakage should be observed under the prevailing operational conditions once the rotational speed has reached a stable state.

Figure 12 presents the comparison between numerical calculations and experimental results for RP seal leakage at rotational speeds in the range of 3000~15,000 $r \cdot min^{-1}$. The leakage rises as the rotational speed increases. The calculation results' maximum error is 11.62%, confirming the LDQ method's accuracy. The main reasons for errors include

two aspects. On one hand, the solved Reynolds equation is a simplification of the Navier–Stokes equation. On the other hand, the inevitable leakage formed at the connection of the test pipeline.

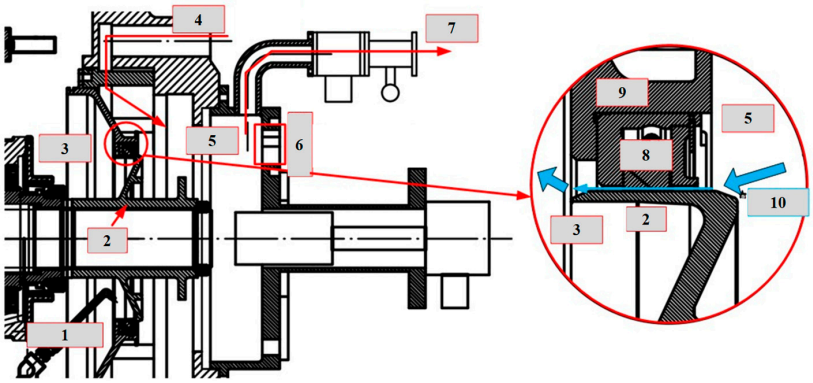

1. Oil nozzle 2. Rotor 3. Low pressure chamber 4. Intake path 5. High pressure chamber 6. Observation window 7. Outflow path 8. Segmented annular seal components 9. Seal casing 10. Leak path

Figure 11. Schematic diagram of leakage testing for the segmented annular seal.

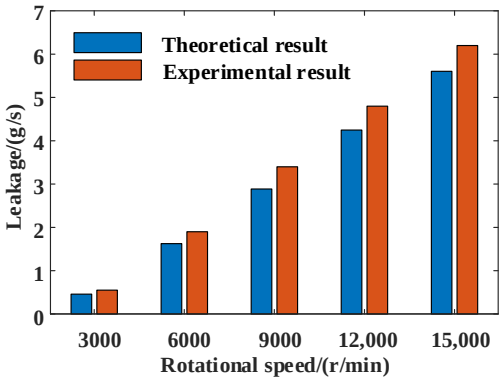

Figure 12. Leakage comparison between theoretical and experimental results (p_0 = 0.1 MPa, *P.R.* = 4).

To further verify the leakage solution accuracy, the segmented annular seal's structure and working parameters in [16] were adopted. The leakage comparison between NASA's results and the LDQ method was depicted in Figure 13. As illustrated in the figure, the simulation leakage result distributes the experimental results on both sides.

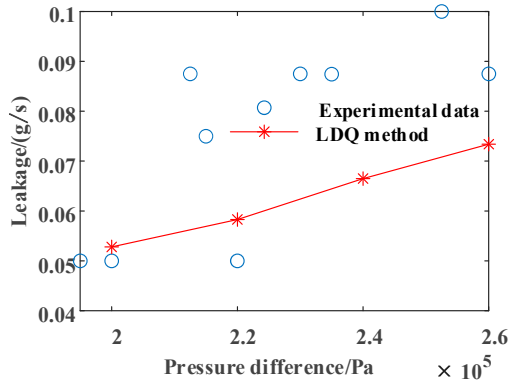

Figure 13. Leakage comparison between LDQ method and [16].

4.3.2. Accuracy Verification of Dynamic Characteristic Solution Method

To confirm the dynamic characteristic solution method accuracy, the same geometric model was established as in [24] for comparison. The comparison result is shown in Table 3.

The maximum deviation of the journal bearing stiffness coefficient and damping coefficient results is less than 10%, which verifies the accuracy of the dynamic characteristic solution model. The deviation arises from different control equations to be solved.

Table 3. Comparison of results from different solution models.

	K (10^6 N/m)	C (10^4 Ns/m)	Deviation of K (%)	Deviation of C (%)
VT-FAST [26]	40.0	5.75	4.25	9.04
DyRoBes [26]	38.0	4.86	9.74	7.61
Differential quadrature method	41.7	5.23	—	—

5. Results and Discussion

5.1. Static Characteristics Results

5.1.1. Distribution of Pressure

Figure 14 illustrates the characteristics of pressure distribution for seals with the RP, the CLCP, and the CPCP without considering the closing force. As illustrated in the figure, the pressure distribution characteristics of the three structural forms of seals are consistent. The pressure field distribution from the high-pressure side to the low-pressure side decreases in a parabolic shape, starting from the circumferential groove's both ends and extending to the segment's both ends. In the axial groove region, the pressure maintains a constant value at the high pressure from the inlet to the downstream boundary of the circumferential groove. A hydrodynamic pressure effect forms at the pocket's circumferential outlet, which creates a localized area of high pressure. From the circumferential groove to the outlet of the computational domain, the pressure decreases linearly. The closer the local high-pressure zone is to the pocket's circumferential outlet, the higher the pressure value is. As the position nears the pocket circumferential outlet, the segmented annular seal circumferential gas film thickness decreases, leading to a more pronounced squeezing of the gas film and a stronger hydrodynamic pressure effect. Compared with the seal with the conventional RP, the one with the CLCP exhibits a 60.94% increase in peak pressure, and the one with the CPCP exhibits an 83.49% increase in peak pressure.

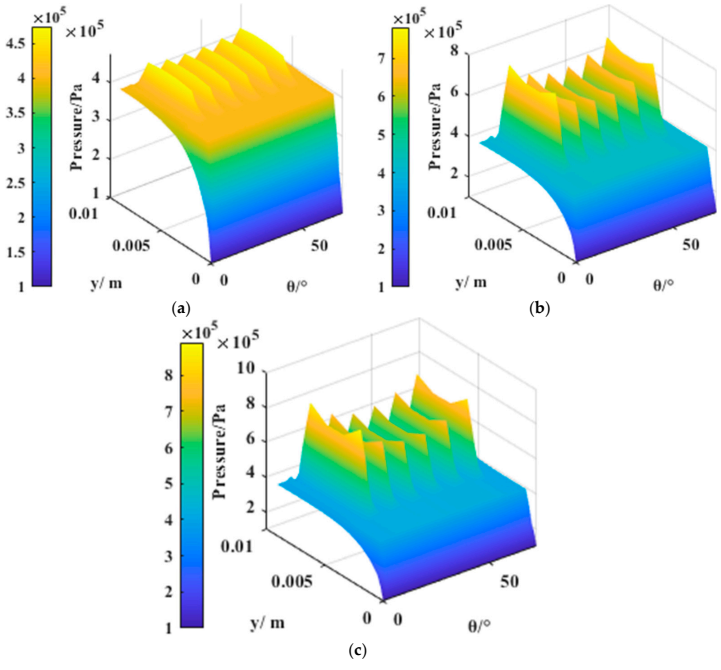

Figure 14. Pressure distribution (p_0 = 0.1 MPa, *P.R.* = 4, n = 15,000 r/min). (**a**) Rectangular pocket. (**b**) Circumferential linear convergent pocket. (**c**) Circumferential parabolic convergent pocket.

The primary cause of the hydrodynamic pressure effect stems from the segmented annular seal fluid source term $\frac{\partial H}{\partial \theta}$ in Equation (4). As the source term increases, the segmented annular seal hydrodynamic pressure effect becomes more pronounced. The $\frac{\partial H}{\partial \theta}$ values of the three types of pocket seals are as follows: along the circumferential direction, the seal with the RP is the smallest, and the seal with the CPCP is the largest.

5.1.2. Leakage

Influence of Operating Parameters on Leakage

Figure 15 illustrates how operating parameters affect seal leakage across three distinct configurations. As the rotational speed and pressure ratio increase, the leakage of the CLCP and CPCP seals rises. In identical operational settings, the leakage of both wedge pocket seals exceeded that of the RP seal. When the rotational speed is within the range of 3000 to 12,000 r/min, the wedge pocket segmented annular seal leakage is 3.49~21.83 g/s. When the pressure ratios range from 3.3 to 3.45, the wedge pocket segmented annular seal leakage is 3.24~11.09 g/s.

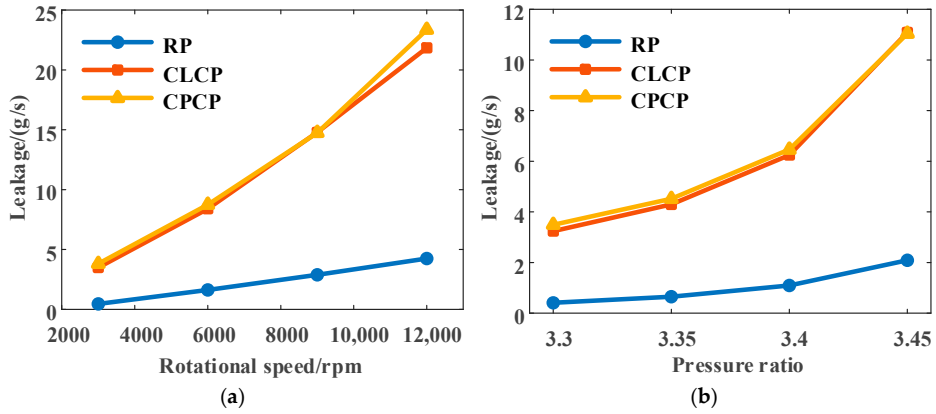

Figure 15. Influence of working conditions on leakage. (**a**) Rotational speed (p_0 = 0.1 MPa, *P.R.* = 4, F_s = 0.36 N). (**b**) Pressure ratio (p_0 = 0.1 MPa, n = 12,000 r/min, F_s = 0.315 N).

The increase in leakage is caused by an increase in the seal clearance, which changes as a result of the combined action of the lift and closing forces. Figure 16 displays the impact of operating conditions on the clearance of the segmented annular seal. All of the three segmented annular seal clearances are observed to increase with an increasing rotational speed. In comparison with the RP seal, the clearances of the CLCP and CPCP seals increase by 73.99% and 79.58%, respectively. At various pressure ratios, the clearances of the CLCP and CPCP seals are larger than that of the RP seal. The wedge pocket can increase the segmented annular seal's clearance under different working conditions.

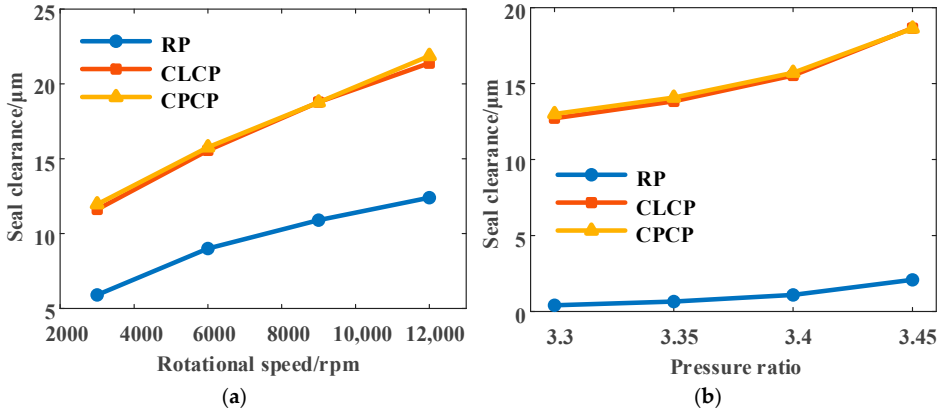

Figure 16. Influence of working conditions on seal clearance. (**a**) Rotational speed. (**b**) Pressure ratio.

Influence of Structural Parameters on Leakage

The results of the influence of operating parameters on the leakage of segmented annular seals with three different structure forms show that the circumferential convergent wedge pocket increases the seal clearance and affects the sealing performance. Consequently, it is necessary to study how circumferential convergent wedge pocket's structural parameters affect the segmented annular seal's leakage.

To evaluate the circumferential convergent wedge pocket's convergence degree, the wedge ratio was defined as shown in Equation (9). An increase in the wedge ratio will result in a corresponding increase in the degree of convergence of the pocket.

$$\gamma = \frac{h_1}{h_2} \tag{9}$$

Figure 17 illustrates the impact of pocket structure parameters on the leakage of the CLCP and the CPCP segmented annular seals under the conditions of a pocket minimum depth of 0.010 mm. It is observed that the leakage of the segmented annular seals of both structural forms increases with an increase in wedge ratio, pocket length, and pocket width. When the wedge ratio is equal to one, the pocket structure form is the conventional RP. The maximum leakage of segmented annular seals is 21.87 g/s under different structural parameters. The average increase in the leakage of the CPCP seal in comparison to the CLCP seal is 8.32%, 11.86%, and 4.72% for various wedge ratios, pocket lengths, and pocket widths.

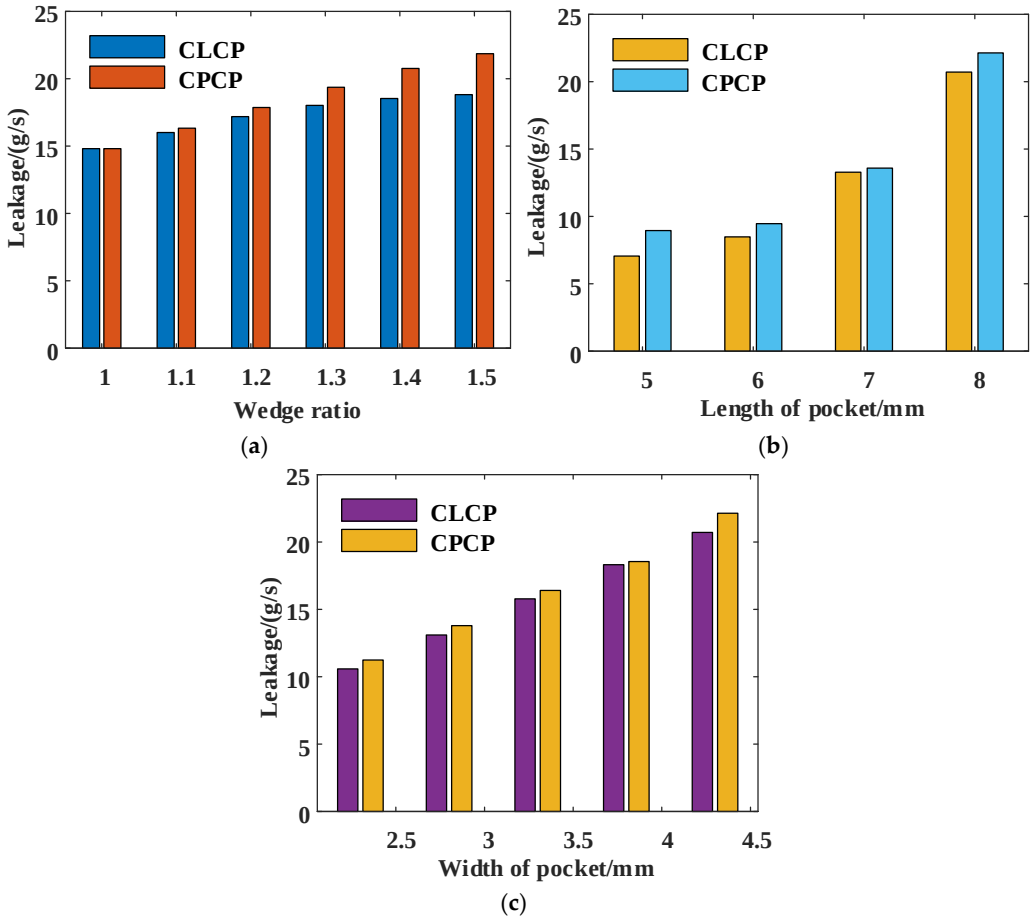

Figure 17. Influence of pocket size on seal leakage (p_0 = 0.1 MPa, *P.R.* = 4, n = 12,000 r/min, F_s = 0.36 N). (**a**) Wedge ratio, (**b**) length of pocket (γ = 2.5), and (**c**) width of pocket (γ = 2.5).

The impact of the structural parameters of the wedge pocket on the segmented annular seal clearance is displayed in Figure 18. As the wedge ratio, pocket length, and pocket width increase, the clearances of the CLCP and the CPCP segmented annular seals increase. Compared to the CLCP segmented annular seal, under different wedge ratios, pocket lengths, and pocket widths, the clearance of the CPCP seal increases by 2.18%, 3.73%, and 1.56%, respectively.

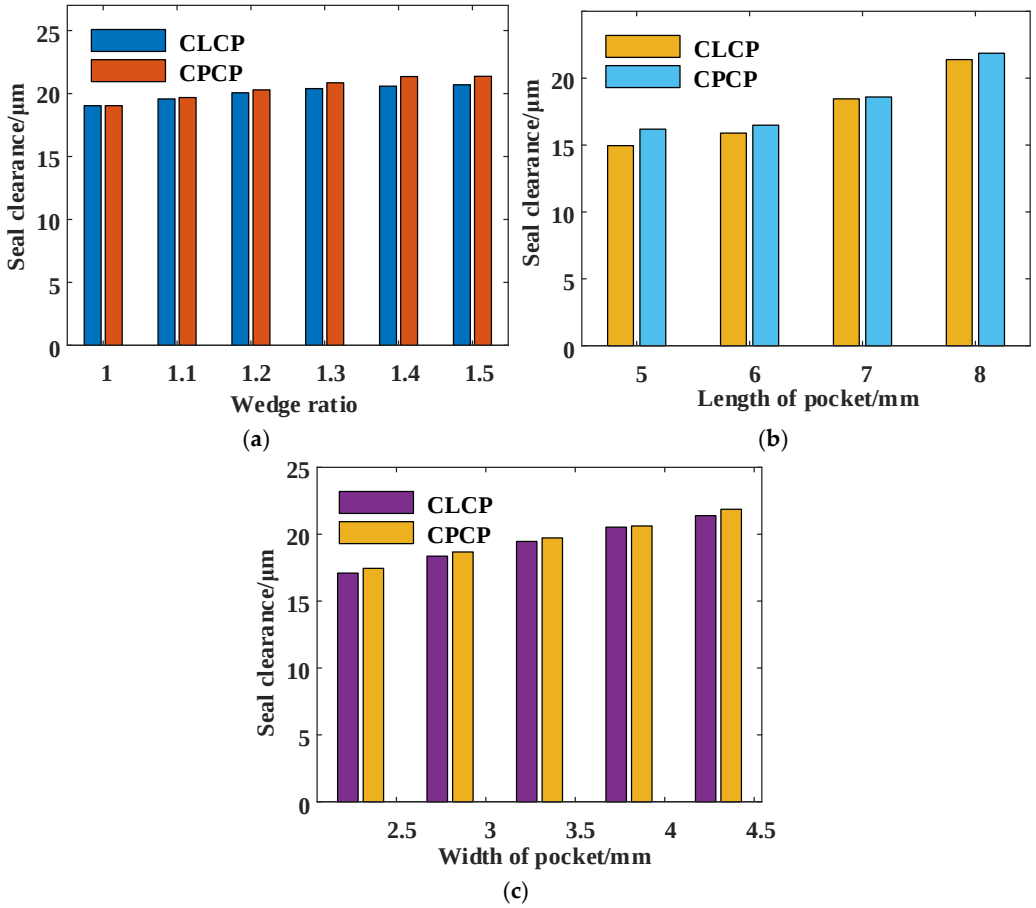

Figure 18. Influence of pocket size on seal clearance, (**a**) wedge ratiol (**b**) length of pocket (γ = 2.5), and (**c**) width of pocket (γ = 2.5).

5.2. Dynamic Characteristics Results

5.2.1. Influence of Operating Parameters on Dynamic Characteristics

Rotational Speed

The influence of rotational speed on the segmented annular seal stiffness and damping coefficients of the three configurations is presented in Figure 19. As the rotational speed rises, the stiffness coefficient and damping coefficient of the seals both decrease. The influence of rotational speed on dynamic characteristics in this article is opposite to the trend in [22], as this article considers the effect of the closing force on the dynamic characteristics of segmented annular seals based on [22]. Under the same working conditions, in comparison to the RP seal, the CLCP seal has an average increase in the stiffness coefficient and damping coefficient of 60.76% and 65.27%, respectively, and the CPCP seal has an average increase of 142.75% and 151.62%, respectively.

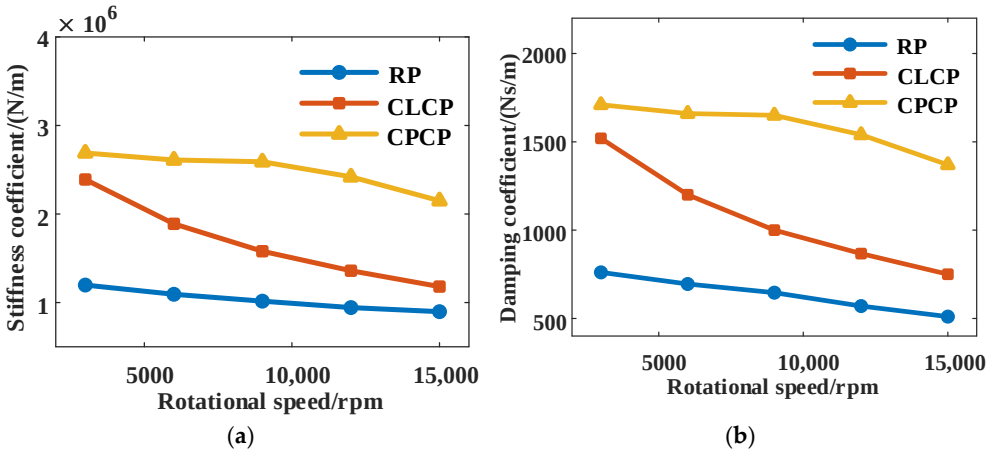

Figure 19. Influence of rotational speed on stiffness and damping coefficients, (**a**) stiffness coefficient, and (**b**) damping coefficient.

Pressure Ratio

The influence of the pressure ratio on the dynamic characteristic coefficients of the segmented annular seals of the three configurations is illustrated in Figure 20. As the pressure ratio rises, the stiffness coefficient and damping coefficient of the seals all decrease. Under the same working conditions, in comparison to the RP seal, the CLCP seal has an average increase of 20.04% in the stiffness coefficient and 19.31% in the damping coefficient. The CPCP seal has an average increase of 77.87% and 73.58%, respectively.

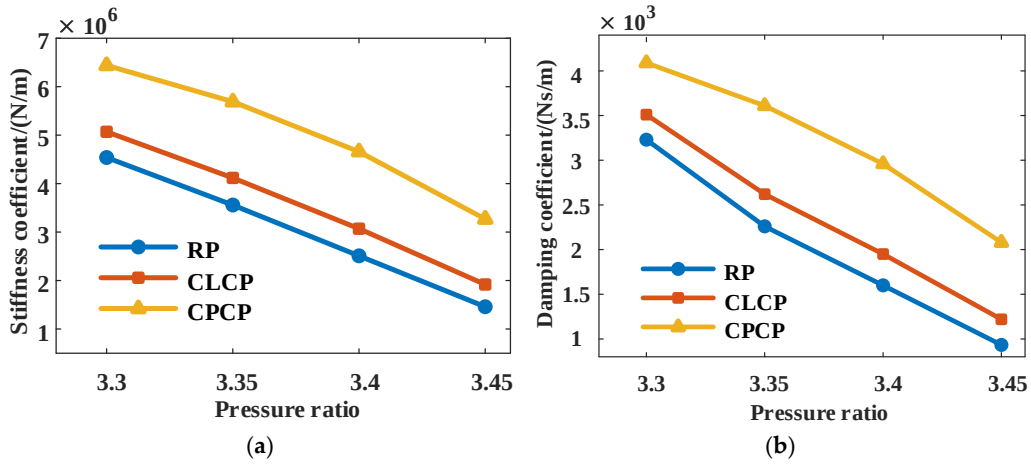

Figure 20. Influence of pressure ratio on dynamic characteristics, (**a**) stiffness coefficient, and (**b**) damping coefficient.

Stability

Figure 21 depicts the influence of working conditions on the damping ratio of the three segmented annular seal configurations. As the rotational speed and pressure ratio increase, the segmented annular seal damping ratios of all three structures is larger than zero, and the system is stable. It has been demonstrated that a conventional RP seal exhibits a damping ratio of less than one at 12,000 and 15,000 r·min^{-1}. Consequently, the system is characterized by an underdamped behavior, and the stability of the system decreases. Under all other operating conditions, the RP seal system is in an overdamped state. The CLCP and the CPCP seals are both overdamped under operating conditions. As a result, both linear and parabolic wedge pockets improve the stability of segmented annular seal systems compared to traditional RPs.

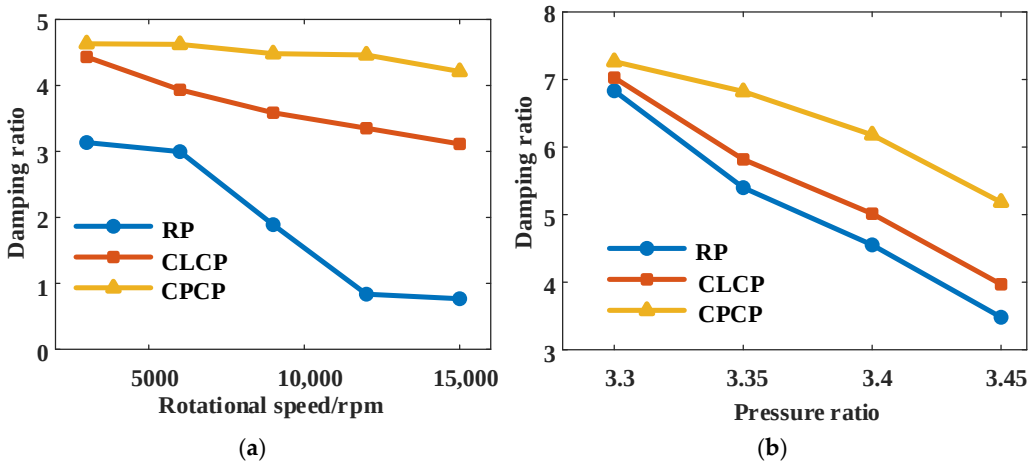

Figure 21. Influence of working conditions on damping ratio, (**a**) rotational speed, and (**b**) pressure ratio.

5.2.2. Influence of Structural Parameters on Dynamic Characteristics

The results of the effects of the operating parameters on the dynamic characteristics of three different structural forms of segmented annular seals show that the circumferential convergent wedge pocket can enhance the stability of the seal. Hence, it is necessary to further investigate the effects of the structural parameters of the circumferential convergent wedge pocket on the dynamic characteristics of segmented annular seals.

Wedge Ratio

Figure 22 shows the impact of the wedge ratio on the CLCP and CPCP seal dynamic characteristics. The stiffness coefficients of the two structures are of the same order of magnitude. Both seals' dynamic characteristic coefficients decrease as the wedge ratio increases. In comparison to the CLCP seal, the CPCP seal demonstrates an average increase of 30.21% in the stiffness coefficient and 24.01% in the damping coefficient, with a more gradual decline. The impact of the wedge ratio on the damping ratio of the CLCP seal in comparison to the CPCP seal is illustrated in Figure 23. As the wedge ratio increases, both segmented annular seal damping ratios decrease and are larger than one, indicating that the system is in a stable state. When the wedge ratio changes, the CPCP seal has a higher damping ratio compared to the CLCP seal.

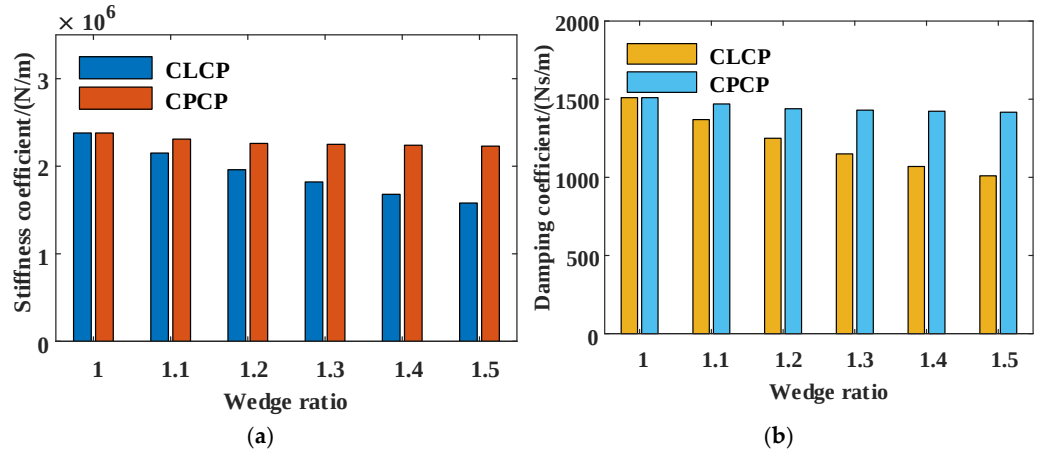

Figure 22. Influence of wedge ratio on dynamic characteristics, (**a**) stiffness coefficient, and (**b**) damping coefficient.

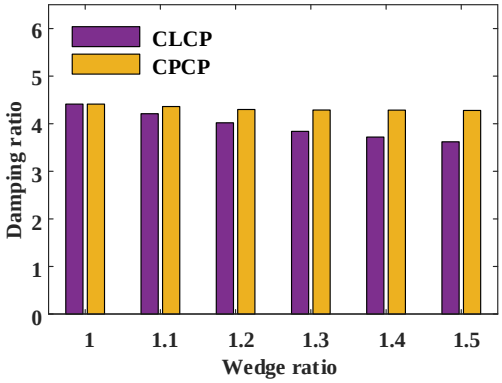

Figure 23. Influence of wedge ratio on damping ratio.

Pocket Length

Figure 24 depicts how pocket length affects the dynamic characteristics of the CLCP and CPCP seal in comparison to the RP seal. It is observed that the seal stiffness and damping coefficients increase for both structural forms with the increasing pocket length. In comparison with the RP seal, the CLCP seal exhibits an average increase of 32.82% in the stiffness coefficient and 39.44% in the damping coefficient, while the CPCP seal exhibits an average increase of 197.25% in the stiffness coefficient and 193.18% in the damping coefficient. The impact of pocket length on the damping ratios of the CLCP and CPCP seals is illustrated in Figure 25. The damping ratios of both seals demonstrate an increase with rising pocket length, reaching values exceeding one. The system is in a state of stability. When the pocket length changes, the CPCP seal has a higher damping ratio compared to the CLCP seal.

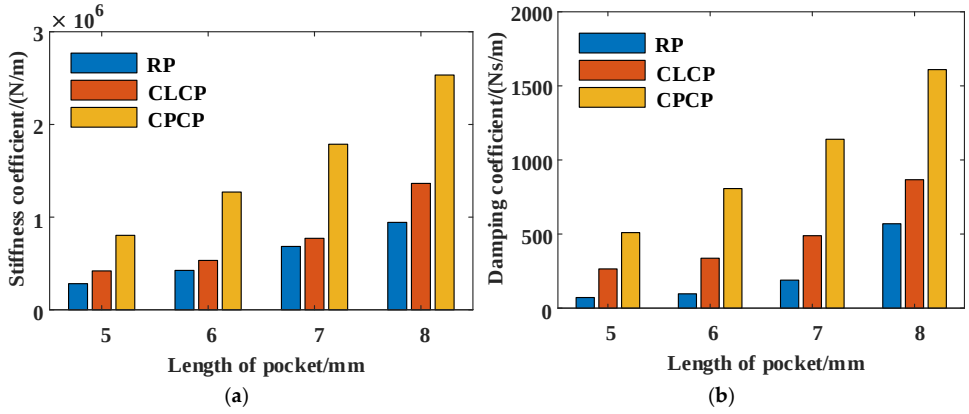

Figure 24. Influence of pocket length on dynamic characteristics, (**a**) stiffness coefficient, and (**b**) damping coefficient.

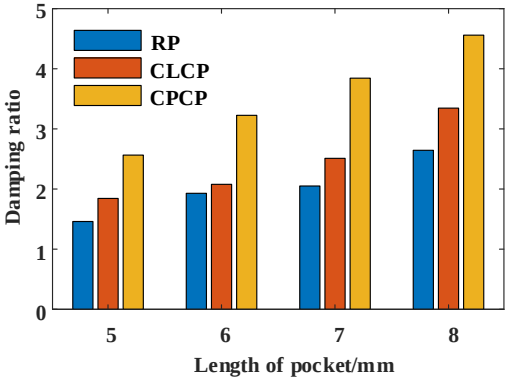

Figure 25. Influence of pocket length on damping ratio.

Pocket Width

Figure 26 depicts how pocket width affects the dynamic characteristics of the CLCP and CPCP seal in comparison to the RP seal. It is observed that the seal stiffness and damping coefficients increase for both structural forms with the increasing pocket width. In comparison with the RP seal, the CLCP seal exhibits an average increase of 42.79% in the stiffness coefficient and 50.71% in the damping coefficient, while the CPCP seal exhibits an average increase of 127.29% in the stiffness coefficient and 142.49% in the damping coefficient. The impact of pocket width on the damping ratios of the CLCP and CPCP seals is illustrated in Figure 27. The damping ratios of both seals demonstrate a decrease with rising pocket width, reaching values exceeding one. The system is in a state of stability. When the pocket width changes, the CPCP seal has a higher damping ratio compared to the CLCP seal.

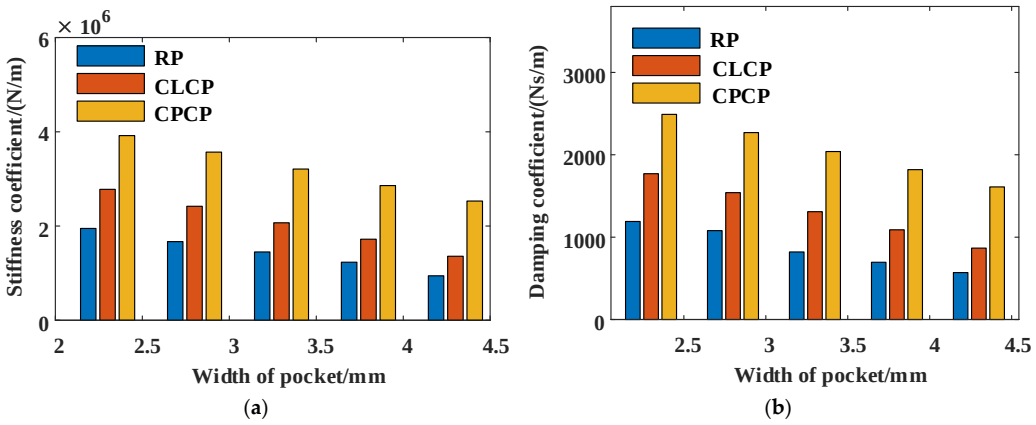

Figure 26. Influence of pocket width on dynamic characteristics, (**a**) stiffness coefficient, and (**b**) damping coefficient.

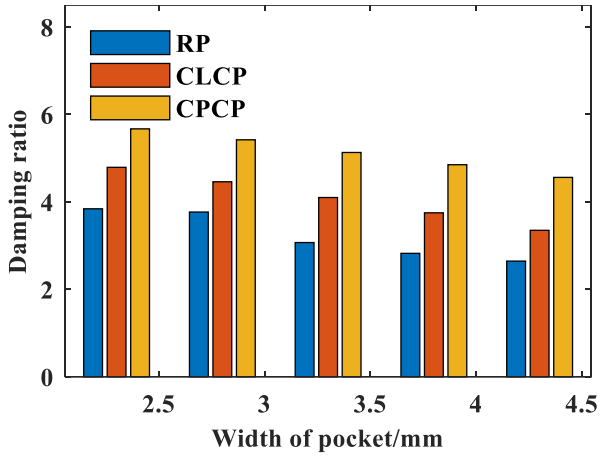

Figure 27. Influence of pocket width on damping ratio.

6. Conclusions

Based on the theory of hydrodynamic lubrication, the CLCP and the CPCP were proposed. The influences of working conditions and wedge pocket parameters on the segmented annular seal's static and dynamic characteristics were analyzed. The key conclusions of the study have been drawn below:

(1) Compared with the conventional RP, the CLCP and the CPCP can notably improve the segmented annular seal's hydrodynamic pressure effect, enlarge the clearances, reduce the friction and improve the problem of poor dynamic characteristics.

(2) With the increase in rotational speed and pressure ratio, the leakage of segmented annular seals with two wedge pocket structures is larger than that of the RP seal. The leakage of both novel seals with circumferentially convergent wedge pocket structures increases with the increase in the wedge ratio, pocket length, and pocket width.

(3) Compared to the traditional RP seal, the CLCP seal has an average increase in the stiffness and damping coefficients of 60.76% and 65.27%, respectively. As the rotational speed increases, the damping ratio of the RP seal decreases, and the seal system transitions from an overdamped state to an underdamped state, resulting in reduced stability. Under different rotational speeds and pressure ratios, both of the CLCP and CPCP seals are in an overdamped state.

(4) A rise in wedge ratio and pocket width is associated with diminished stiffness and damping coefficients in both CLCP and CPCP seals, while an increase in pocket length results in improved dynamic characteristics. In this study, when the static and dynamic characteristics of the seals are taken into account, the CLCP seal is identified as the most optimal structure.

The research content of this article provides new ideas for the optimization design of segmented annular seal structures, which is expected to stimulate more structural optimization of segmented annular seal structures for static and dynamic characteristics. The next stage will investigate the influence of temperature on the static and dynamic characteristics of circular graphite seals.

Author Contributions: Conceptualization, S.W., D.S. and H.Z.; Software, S.W.; Validation, S.W.; Formal analysis, S.W.; Resources, D.S.; Data curation, S.W.; Writing—original draft, S.W.; Writing—review & editing, D.S., Z.Y. and W.X.; Visualization, S.W.; Supervision, D.S.; Project administration, D.S.; Funding acquisition, D.S. and H.Z. All authors have read and agreed to the published version of the manuscript.

Funding: National Natural Science Foundation of China (Grant Nos. 52375195 and 52475206), Fundamental research funds for universities of liaoning province (Grant No. 20240241).

Data Availability Statement: Data will be made available on request.

Conflicts of Interest: The authors declare that they have no known competing financial interests or personal relationships that could have appeared to influence the work reported in this paper.

References

1. Dahite, S.; Arghir, M. Thermogasodynamic analysis of the segmented annular Seal. *ASME J. Tribol.* **2021**, *143*, 072301. [CrossRef]
2. Bai, S.X.; Chu, D.; Ma, C.H.; Yang, J.; Bao, S.Y. Thermo-hydrodynamic effect of gas split floating ring seal with Rayleigh step grooves. *Materials* **2023**, *16*, 2283. [CrossRef] [PubMed]
3. He, Z.P.; Jia, L.H.; Si, J.X.; Li, N.; Wang, H.Y.; Li, B.C.; Guo, Y.H.; Zhao, S.J.; Luo, W.D. Research on the sealing performance of segmented annular seals based on fluid–solid–thermal coupling model. *Lubricants* **2024**, *12*, 407. [CrossRef]
4. Li, G.Q.; Zhang, S.; Kang, Z.; Zhang, Y.F.; Lu, X.G.; Zhu, J.Q. Leakage and wear characteristics of carbon seals for aero-engines. *Chin J. Aeronaut.* **2022**, *35*, 389–400. [CrossRef]
5. Burcham, R.E. *Segmented, Arch-Bound Carbon Seal Is Pressure Loaded*; Report No.: B67-10325; NASA: Washington, DC, USA, 1967. Available online: https://ntrs.nasa.gov/search.jsp?R=19670000325 (accessed on 23 February 2025).
6. Burcham, R.E. *Liquid Rocket Engine Turbopump Rotating-Shaft Seals*; National Aeronautics and Space Administration: Washington, DC, USA, 1978.
7. Pescosolido, A.; Dobek, L. Development of high misalignment carbon seals. In Proceedings of the 37th Joint Propulsion Conference and Exhibit, Salt Lake City, UT, USA, 8–11 July 2001.
8. Ludwig, L.P.; Lynwander, P. *Mainshaft Seals for Small Gas Turbine Engines*; National Aeronautics and Space Administration: Washington, DC, USA, 1974.
9. Yang, H.W.; Bai, S.X. Gas hydrodynamic lubrication performance of split floating ring seals with Rayleigh step grooves. *J. Propuls. Technol.* **2022**, *43*, 148–154. [CrossRef]

10. Arghir, M.; Mariot, A. Theoretical analysis of the static characteristics of the carbon segmented seal. *ASME J. Tribol.* **2017**, *139*, 062202. [CrossRef]
11. Michaelis, S. Contaminated aircraft cabin air. *J. Biol. Phys. Chem.* **2011**, *11*, 132–145. [CrossRef]
12. Zhang, F.Y.; Yang, J.M.; Shui, H.C.; Dong, C.C. Effect of roughness on sealing performance of oil seals with surface texture. *Ind. Lubr. Tribol.* **2020**, *72*, 525–532. [CrossRef]
13. Goldring, E.N. *Feasibility Study of Negative Lift Circumferential Type Seal for Helicopter Transmissions*; Report No.: CR-135302; NASA: Washington, DC, USA, 1977. Available online: https://ntrs.nasa.gov/citations/19780009447 (accessed on 23 February 2025).
14. Allen, G.P. *Self-Acting Lift-Pad Geometry for Circumferential Seals: A Noncontacting Concept*; National Aeronautics and Space Administration: Washington, DC, USA, 1980. Available online: https://ntrs.nasa.gov/citations/19800006146 (accessed on 23 February 2025).
15. Burcham, R.E.; Diamond, W.A. *High-Pressure Hot-Gas Self-Acting Floating Ring Shaft Seal for Liquid Rocket Turbopumps*; National Aeronautics and Space Administration: Washington, DC, USA, 1980. Available online: https://ntrs.nasa.gov/citations/19810017923 (accessed on 23 February 2025).
16. Strom, T.N.; Ludwig, L.P. *Development of Circumferential Seal for Helicopter Transmission Result of Bench and Flight Tests*; National Aeronautics and Space Administration: Washington, DC, USA, 1975. Available online: https://ntrs.nasa.gov/citations/19750024982 (accessed on 23 February 2025).
17. Kikuchi, M.; Oike, M.; Watanabe, Y.; Nosaka, M. *Durability of a Carbon Segmented Circumferential Seal for a Liquid Oxygen Turbopump*; National Aerospace Laboratory: Bangalore, India, 1992.
18. Oike, M.; Nosaka, M.; Watanabe, Y.; Kikuchi, M.; Kamijo, K. Experimental study on high-pressure gas seals for a liquid oxygen turbopump. *Tribol. Trans.* **1988**, *31*, 91–97. [CrossRef]
19. Yuri, K.; Izhak, E. Analysis of the hydrodynamic effects in a surface textured circumferential gas seal. *Tribol. Trans.* **2001**, *44*, 472–478. [CrossRef]
20. Wang, S.; Zhao, H.; Dan, S.; Xu, W.F. Theoretical analysis of gas hydrodynamic lubrication in a carbon segmented seal with the local Differential Quadrature-Lagrange method. In Proceedings of the 2023 International Symposium on Clean Energy and Advanced Materials, Hangzhou, China, 17–19 February 2023.
21. Dahite, S.; Arghir, M. Numerical modelling of a segmented annular seal with enhanced lift effects. *Mech. Syst. Signal Process.* **2021**, *152*, 107455. [CrossRef]
22. Wang, S.; Sun, D.; Yang, Z.M.; Xu, W.F.; Zhao, H.; Wen, S.F. Investigation of static and dynamic characteristics of the segmented annular seals based on the differential quadrature method. *Tribol. Int.* **2024**, *196*, 109657. [CrossRef]
23. Li, G.Q.; Zhu, J.Q.; Xu, G.; Lu, X.G.; Zhang, Y.F. A Graphite Sealing Structure with Anti-Fishbone Dynamic Pressure Groove. CN 111927633A, 20 August 2020.
24. Li, G.Q.; Zhu, J.Q.; Xu, G.; Lu, X.G.; Zhang, Y.F. A Graphite Sealing Structure with Diagonal Dynamic Pressure Grooves. CN 111927635A, 20 August 2020.
25. Sun, D.; Wang, S.; Fei, C.W.; Ai, Y.T.; Wang, K.M. Numerical and experimental investigation on the effect of swirl brakes on the labyrinth seals. *ASME J. Eng. Gas Turbines Power* **2016**, *138*, 032507. [CrossRef]
26. Guo, Z.L.; Hirano, T.; Kirk, R.G. Application of CFD analysis for rotating machinery-Part I: Hydrodynamic, hydrostatic bearings and squeeze film damper. *ASME J. Eng. Gas Turbines Power* **2005**, *127*, 445–451. [CrossRef]

Disclaimer/Publisher's Note: The statements, opinions and data contained in all publications are solely those of the individual author(s) and contributor(s) and not of MDPI and/or the editor(s). MDPI and/or the editor(s) disclaim responsibility for any injury to people or property resulting from any ideas, methods, instructions or products referred to in the content.